

High-rate transmission scheme for pulse-based ultra-wideband systems over dense multipath indoor channels

H. Liu

Abstract: A new high-rate transmission scheme is proposed for pulse-based ultra-wideband (UWB) systems over dense multipath channels. In contrast to the existing UWB schemes that transmit one short-duration pulse each pulse-repetition interval, the proposed scheme transmits a series of N ($N \geq 1$) consecutive pulses (a burst) each burst-repetition interval. The author then develops a successive, a zero-forcing (ZF), and a high-performance ZF-based successive receiver for effective detection in the presence of intersymbol interference within a burst. To lower complexity, an efficient algorithm for the ZF-based successive receiver is also derived. The error performance of these receivers, assuming the availability of perfect channel estimates over lognormal fading channels, is studied. Comparison is made between the proposed scheme and the conventional pulse amplitude-modulation scheme, when the transmission rate, the total transmitted power, and the channel delay spread are kept the same. Impacts of imperfect channel estimation are also studied by simulation. The proposed scheme could achieve a much higher throughput than the conventional scheme in dense multipath channels.

1 Introduction

The commonly used signalling scheme for pulse-based ultra-wideband (UWB) systems [1–10] transmits one short-duration, low-duty-cycle pulse every pulse-repetition interval (PRI). Such a UWB system is capable of high-speed transmission over short distances (e.g. a few metres) in line-of-sight (LOS) propagation environments. For communications in non-LOS (NLOS) dense multipath environments, however, multipath delay could severely limit the maximum data rate (inverse of the minimum PRI for binary signalling) because the adjacent pulses must be sufficiently separated in time to avoid severe intersymbol interference (ISI). The typical root-mean-square (RMS) delay spread τ_{rms} in indoor environments ranges from 17 to 40 ns for antenna separations from 5 to 30 m [11]. For this range of delay spread values of the channel, the achievable maximum data rate could be very low. Observations on data rate limits of pulsed UWB systems over dense multipath channels have been made in [2]. One of the major objectives of recent proposals on multi-band (OFDM) UWB systems [12] is to improve the link throughput. OFDM is a recognised multicarrier solution to combat the effects of multipath conditions, especially for high-rate communications, because a complex adaptive equaliser is not needed. However, OFDM suffers from a number of problems such as sensitivity to the carrier-frequency offset, phase noise and a high peak-to-average power ratio [13]. Additionally, multi-band OFDM UWB systems are in general more complex than the pulsed systems.

In this paper, a new scheme for high-rate transmission in pulse-based UWB systems is proposed. In the proposed scheme, a series of N ($N \geq 1$) consecutive pulses (a burst) are transmitted in each burst-repetition interval (BRI). The BRI can be made large enough for the range of delay spread values encountered to avoid inter-burst interference (IBI). However, adjacent pulses within a burst cause severe ISI. A successive, a zero-forcing (ZF) and a high-performance ZF-based successive receiver are then proposed for effective detection in the presence of ISI within a burst. A computationally efficient algorithm is also derived for the ZF-based successive receiver to reduce its complexity. Because the amplitude of indoor channels has been shown to have a lognormal distribution [9, 11] rather than the well addressed Rayleigh distribution, the error performance of these receivers over lognormal fading channels is provided. A performance comparison is made between the proposed scheme and the conventional pulse amplitude modulation (PAM) scheme.

2 System model

The commonly used binary PAM scheme for a pulse-based UWB system is illustrated in Fig. 1, where the amplitude of short-duration pulses is modulated by information bits. For a general PAM scheme, the transmitted signal is expressed

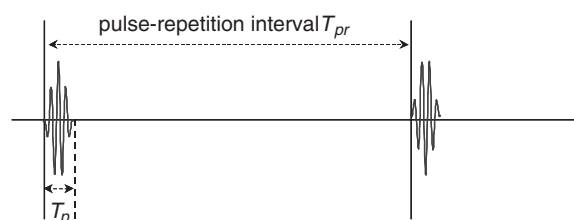


Fig. 1 Commonly used UWB PAM (antipodal) signalling scheme

© IEE, 2005

IEE Proceedings online no. 20040648

doi:10.1049/ip-com:20040648

Paper first received 11th December 2003 and in revised form 15th April 2004

The author is with the School of Electrical Engineering and Computer Science, Oregon State University, Corvallis, OR 97331, USA

as

$$x(t) = \sum_{i=-\infty}^{\infty} \sqrt{E_p} s(i) p(t - iT_{pr})$$

where $p(t)$ is the UWB pulse shape, $s(i)$ is the i th symbol, E_p represents the energy per pulse and T_{pr} denotes the pulse-repetition interval. In order to avoid partial correlation of the received pulses, it is assumed that $p(t)$ is non-zero only in the interval $0 \leq t \leq T_p$ and the minimum path resolution is equal to the pulse duration [2].

The proposed new high-rate transmission scheme is illustrated (binary signalling is used again) in Fig. 2, where a burst of N consecutive pulses is transmitted at the beginning of each burst-repetition interval. The transmitted signal is expressed as

$$x(t) = \sum_{i=-\infty}^{\infty} \sum_{n=1}^N \sqrt{E_p} s_n(i) p(t - iT_r - nT_p) \quad (1)$$

where $s_n(i)$ is the n th symbol of the i th burst, T_r represents the burst-repetition interval and T_p is the pulse duration. The energy of $p(t)$ is normalised as $\int_{-\infty}^{\infty} p^2(t) dt = 1$. In order to minimise inter-burst interference, the guard time between adjacent bursts ($T_r - NT_p$) must be large enough for the range of delay-spread values encountered. This constraint determines the maximum number of symbols per burst that can be transmitted for a specific value of the channel delay spread and T_r . If all symbols in one burst can be successfully detected, the transmission rate of the proposed scheme is N/T_r . If the guard intervals between adjacent pulses in the conventional system ($T_{pr} - T_p$) and between adjacent bursts in the proposed system ($T_r - NT_p$) are kept the same, the ratio of the transmission rates of the proposed scheme to the conventional scheme is

$$\beta = \frac{NT_{pr}}{T_r} = N - \frac{N(N-1)T_p}{T_r}$$

For example, with $T_p = 0.2$ ns, $T_r = 40$ ns and $N = 5$, the ratio is $\beta = 4.9$.

A UWB channel is a highly frequency-selective channel, whose impulse response may be modelled as [2, 11]

$$c(t) = \sum_{l=0}^{L-1} h(l) \delta(t - lT_p) \quad (2)$$

where $h(l)$ represents the fading coefficient of the l th resolvable path, L is the total number of resolvable multipath components and $\delta(t)$ is the Dirac delta function. UWB systems are mostly for indoor applications, and indoor channels have been shown to have lognormal amplitude fading statistics [9, 11]. The UWB-channel model adopted in [2, 9] suggests that $h(l) = \theta(l)\alpha(l)$, where $\alpha(l)$ is a lognormally distributed random variable (RV) and $\theta(l)$ with an equal probability to take on the value of 1 or -1 , accounts for the random-pulse inversion that could occur

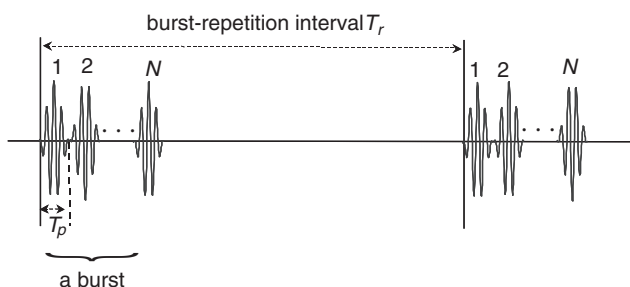


Fig. 2 Proposed new high-rate UWB PAM signalling scheme

due to reflections. The average power of the channel decays exponentially [11]. Thus, the power of the l th path can be modelled as $E\{|h(l)|^2\} = \Omega_0 e^{-\rho l}$, where $E\{\cdot\}$ denotes the statistical expectation, ρ is the power decay factor and Ω_0 can be used to adjust the power of the path with the index $l = 0$.

3 Receiver

3.1 Received signal

Given the transmitted signal $x(t)$ in (1) and the channel modelled by (2), the received signal is expressed as

$$r(t) = \sum_{l=0}^{L-1} h(l)x(t - lT_p) + v(t) \quad (3)$$

where $v(t)$ is the received additive white Gaussian noise (AWGN) with a two-sided spectral density $N_0/2$.

The received signal is filtered by a matched filter, which is matched to $p(t)$, and then sampled at the pulse rate. With the channel model adopted, the resolvable multipath components are shifted relative to one another by integer multiples of T_p (minimum multipath resolution). Therefore, in the first pulse interval of a burst, the receiver receives only the first transmitted symbol of that burst. In the second pulse interval of a burst, the receiver receives the sum of the signals transmitted in the first and the second pulse intervals, each arriving via an independently faded channel, and so on. Thus, in the absence of inter-burst interference, the first M ($M \geq N$) samples in i th burst of the matched filter output can be written in an $M \times 1$ vector as

$$\mathbf{r} = [r_1, r_2, \dots, r_M]^T = \sqrt{E_p} \mathbf{H} \mathbf{s} + \mathbf{v} \quad (4)$$

where index i (represents the i th burst) is omitted for simplicity of notation, $[\cdot]^T$ denotes transpose, $\mathbf{s} = [s_1, s_2, \dots, s_N]^T$ is the symbol vector transmitted in the i th burst and \mathbf{H} is the $M \times N$ channel matrix given as

$$\mathbf{H} = \begin{bmatrix} h(0) & 0 & 0 & \dots & 0 \\ h(1) & h(0) & 0 & \dots & 0 \\ h(2) & h(1) & h(0) & \dots & 0 \\ \vdots & \vdots & \vdots & \ddots & \vdots \\ h(M-1) & h(M-2) & \dots & \dots & h(M-N) \end{bmatrix} \quad (5)$$

The noise component \mathbf{v} is an $M \times 1$ zero-mean Gaussian vector with independent and identically distributed elements. Thus, $E\{\mathbf{v}\mathbf{v}^H\} = (N_0/2)\mathbf{I}_M$ where $(\cdot)^H$ denotes conjugate transpose [Note 1] and \mathbf{I}_M is the $M \times M$ identity matrix. For effective reception, the number of samples (M) must be greater than or equal to N , the number of symbols transmitted in each burst.

3.2 Successive receiver

It is easy to see from (4) and (5) that the first sample of the received signal (r_1) carries the first symbol of each burst. The second sample (r_2) carries the sum of the first and second symbols of a burst, and so on. In the successive receiver, the first symbol of a burst is detected using r_1 only. In deriving the receiver, we assume the availability of perfect knowledge of the channel matrix \mathbf{H} . In Section 4, we will simulate the impact of imperfect channel estimates. Let the decision for s_1 be $\hat{s}_1 = Q(r_1/h(0))$, where $Q(\cdot)$ denotes the quantisation operation appropriate for the signal constellation chosen.

Note 1: Noise is real with the system model and the channel model adopted in this paper. The notation of conjugate transpose is still used here because of its mathematical convenience.

The second symbol s_2 is detected by slicing $(r_2 - \sqrt{E_p}\hat{s}_1 / \{\mathcal{H}\}_{21})/h(0)$ as $\hat{s}_2 = Q((r_2 - \sqrt{E_p}\hat{s}_1[\mathcal{H}]_{21})/h(0))$, where $[\mathcal{H}]_{21}$ is the (2, 1)th element of \mathcal{H} . To generalise, the n th symbol of each burst is detected as

$$\hat{s}_1 = Q(r_1/h(0)) \quad (6a)$$

$$\hat{s}_n = Q\left(\left(r_n - \sum_{u=1}^{n-1} \sqrt{E_p}\hat{s}_u[\mathcal{H}]_{nu}\right) \frac{1}{h(0)}\right), \quad (6b)$$

$n = 2, \dots, N$

This receiver needs only the first N samples (the 1st to the N th pulse intervals) to detect all symbols of each burst.

The successive receiver is simple. However, it neither provides a diversity gain nor combines the energy contained in multiple resolvable paths. Also, the $(n+1)$ th symbol of a burst has a slightly worse performance than the n th symbol of a burst because of the error propagation introduced in the interference-cancellation process.

3.3 Zero-forcing receiver

A zero-forcing (ZF) scheme can be applied for effective detection in the proposed UWB scheme. In the ZF receiver, the received signal given in (4) is pre-multiplied by the pseudoinverse of \mathcal{H} , resulting in the $N \times 1$ zero-forced signal as

$$\begin{aligned} \mathbf{y} &= [y_1, y_2, \dots, y_N]^T \\ &= \mathcal{H}^+ \mathbf{r} = \sqrt{E_p} \mathbf{s} + \boldsymbol{\xi} \end{aligned} \quad (7)$$

where $(\cdot)^+$ denotes the pseudoinverse of a matrix and $\boldsymbol{\xi} = \mathcal{H}^+ \mathbf{v}$ ($N \times 1$) is the real Gaussian noise component at the output of the ZF receiver. Decisions of all symbols in each burst can be obtained by passing each element of \mathbf{y} independently through a decision device (i.e. $\hat{s} = Q(\mathbf{y})$). Because an overdetermined system ($M \geq N$) is considered, \mathcal{H}^+ can be obtained as $\mathcal{H}^+ = (\mathcal{H}^H \mathcal{H})^{-1} \mathcal{H}^H$.

One problem with applying the ZF receiver to the proposed scheme is the noise enhancement due to the zero-forcing operation. Conditioned on a fixed-channel matrix, the instantaneous covariance matrix of the zero-mean noise vector at the output of the ZF receiver is determined to be $\mathbf{R}_\xi = E\{\boldsymbol{\xi}\boldsymbol{\xi}^H\} = E\{\mathcal{H}^+ \mathbf{v} \mathbf{v}^H \mathcal{H}^{+H}\} = (N_0/2) \mathcal{H}^+ \mathcal{H}^{+H}$. For $M \geq N$, it is easy to show that $\mathbf{R}_\xi = (N_0/2)(\mathcal{H}^H \mathcal{H})^{-1}$. Thus, the instantaneous noise enhancement factor for the n th symbol of a burst is $[(\mathcal{H}^H \mathcal{H})^{-1}]_{nn}$, where $[\cdot]_{nn}$ denotes the (n, n) th element. Another problem with applying the ZF receiver to the proposed scheme is that the average noise enhancement varies for different symbols of a burst. The first symbol, being present in all received samples, has an

obvious advantage over all other symbols, and the last symbol of a burst has the worst performance. This problem can be alleviated by exploiting more resolvable paths in the receiver. The larger the number of paths exploited, the less the noise enhancement and the smaller the performance gap among different symbols of a burst. When the number of paths exploited by the receiver is greater than N , an implicit diversity gain is also provided by the ZF receiver.

3.4 Zero-forcing-based successive receiver

To overcome the shortcomings of the ZF and the successive receivers, we derive a ZF-based successive receiver. A block diagram of this receiver is shown in Fig. 3. As mentioned earlier, in a ZF receiver the first symbol has the best error performance. In the proposed receiver, the first symbol of each burst, s_1 , is detected by slicing the first element of $\mathcal{H}^+ \mathbf{r}$. This is the same as the ZF receiver and let the detected symbol be \hat{s}_1 . When $M > N$, \hat{s}_1 obtained this way will be much more reliable than that obtained by the successive receiver because of the implicit diversity gain through the ZF receiver.

A reduced-dimension received signal vector, $\mathbf{r}_{(2)}$, is then formed as

$$\begin{aligned} \mathbf{r}_{(2)} &= [r_2 - \sqrt{E_p}h(1)\hat{s}_1, r_3 - \sqrt{E_p}h(2)\hat{s}_1, \dots, r_M \\ &\quad - \sqrt{E_p}h(M-1)\hat{s}_1]^T \end{aligned} \quad (8)$$

If \hat{s}_1 is a correct decision, then $\mathbf{r}_{(2)}$ can be expressed as

$$\mathbf{r}_{(2)} = \sqrt{E_p} \mathcal{H}_{(2)} \mathbf{s}_{(2)} + \mathbf{v}_{(2)} \quad (9)$$

where $\mathbf{s}_{(2)} = [s_2, s_3, \dots, s_M]^T$, $\mathbf{v}_{(2)} = [v_2, v_3, \dots, v_M]^T$, and $\mathcal{H}_{(2)}$ is formed by deleting the first column and the first row of \mathcal{H} . The second symbol of each burst, s_2 , is detected by slicing the first element of $\mathcal{H}_{(2)}^+ \mathbf{r}_{(2)}$. After that, a reduced-dimension vector, $\mathbf{r}_{(3)}$, and matrix, $\mathcal{H}_{(3)}$, are formed based on $\mathbf{r}_{(2)}$ and $\mathcal{H}_{(2)}$ using the same procedure. Symbol s_3 is detected by slicing the first element of $\mathcal{H}_{(3)}^+ \mathbf{r}_{(3)}$, and this procedure continues until s_N is detected.

In detecting s_2 , the pseudoinverse of a reduced-size $((M-1) \times (N-1))$ matrix $\mathcal{H}_{(2)}$ is needed. In forming $\mathcal{H}_{(2)}$, the row and column of \mathcal{H} that do not carry information of s_2 are deleted. The diversity for detecting s_2 is still implicitly provided through this procedure. It is generally true that the smaller the size of the matrix to be inverted, the less the noise enhancement it will introduce. Thus, noise enhancement to detect s_2 by this receiver is lower than in the normal ZF scheme. The same is true for all other symbols s_3, \dots, s_N .

This receiver seems to be significantly more complex than the ZF or the successive receiver; detection of s in one burst

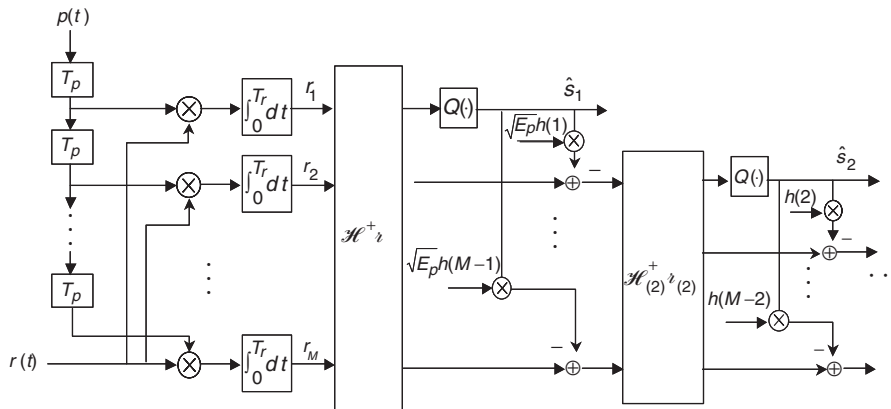


Fig. 3 ZF-based successive detector

requires the pseudoinverse of $N-1$ channel matrices of size $M \times N$ to size $(M-N+2) \times 2$. However, the computational needs associated with inverting the $N-1$ matrices can be dramatically reduced by exploiting an efficient algorithm. As mentioned earlier in this Section, \mathcal{H}^+ can be obtained as $\mathcal{H}^+ = (\mathcal{H}^H \mathcal{H})^{-1} \mathcal{H}^H$. If \mathcal{H}^+ has been initially computed, then the algorithm allows the inversion of matrices $\mathcal{H}_{(2)}, \dots, \mathcal{H}_{(N)}$ to be obtained recursively from \mathcal{H}^+ , without actually inverting these matrices. Let

$$\mathbf{G}_N = \mathcal{H}^H \mathcal{H} = \begin{bmatrix} g_{00} & \mathbf{g}_{01}^T \\ \mathbf{g}_{10} & \mathbf{G}_{N-1} \end{bmatrix} \quad (10a)$$

$$\mathbf{D}_N = \mathbf{G}_N^{-1} = \begin{bmatrix} d_{00} & \mathbf{d}_{01}^T \\ \mathbf{d}_{10} & \mathbf{D}_{N-1} \end{bmatrix} \quad (10b)$$

where g_{00} is the (1,1)th element of \mathbf{G}_N and d_{00} is the (1, 1)th element of \mathbf{D}_N . From the identity $\mathbf{G}_N \mathbf{D}_N = \mathbf{I}_N$, the following equations are easily obtained:

$$g_{10} d_{00} + \mathbf{G}_{N-1} \mathbf{d}_{10} = \mathbf{0}_{(N-1) \times 1} \quad (11a)$$

$$g_{10} \mathbf{d}_{01}^T + \mathbf{G}_{N-1} \mathbf{D}_{N-1} = \mathbf{I}_{N-1} \quad (11b)$$

From (11a) and (11b), an important relationship is obtained as

$$\mathbf{G}_{N-1}^{-1} = \mathbf{D}_{N-1} - \mathbf{d}_{10} \mathbf{d}_{01} d_{00}^{-1} \quad (12)$$

where d_{00} is a scalar. Equation (12) states that if inversion of the $N \times N$ matrix $\mathbf{G}_N = \mathcal{H}^H \mathcal{H}$ has been obtained in computing \mathcal{H}^+ , inversions of all other matrices ($\mathbf{G}_{N-1} = \mathcal{H}_{(2)}^H \mathcal{H}_{(2)}, \dots, \mathbf{G}_2 = \mathcal{H}_{(N-1)}^H \mathcal{H}_{(N-1)}$) needed for the detection can be computed recursively using the relationship given by (12). Thus, to detect all symbols in each burst, this receiver needs to invert only one matrix of size $N \times N$, and its complexity is approximately $O(N^3)$ plus the multiplication of $(\mathcal{H}^H \mathcal{H})^{-1}$ and \mathcal{H}^H (additional computation in applying (12) is negligible). Therefore, the ZF-based successive receiver has a complexity that is approximately equal to that of the ZF receiver, but it should provide a much better overall error performance.

4 Simulation results and discussion

For all simulations, the average power of $h(0)$ is normalised to 1 (i. e. $\Omega_0 = 1$). The lognormally distributed random variable (RV) $\alpha(l)$ can be expressed as $\alpha(l) = e^{z(l)}$ where $z(l)$ is a Gaussian RV with a mean $\mu_{z(l)}$ and variance $\sigma_{z(l)}^2$. The standard deviation of $20 \log_{10} \alpha(l) = z(l)(20 \log_{10} e)$, which typically ranges from 3 to 5 dB for indoor communications [2], is independent of the multipath index l . Thus, we can write $\sigma_{z(l)} = \sigma_z$. The k th moment of the lognormal RV $\alpha(l)$ is given as

$$E\{\alpha(l)^k\} = e^{(k\mu_{z(l)} + k^2\sigma_{z(l)}^2/2)}$$

To satisfy $E\{\alpha(l)^2\} = e^{-pl}$, it is required that $\mu_{z(l)} = -\sigma_z^2 - pl/2$. In generating channel coefficients $\alpha(l) = e^{z(l)}$, a 4-dB standard deviation for $z(l)(20 \log_{10} e)$ is chosen. With this parameter, $\mu_{z(l)}$ and $\sigma_{z(l)}$ can be calculated. The total number of resolvable multipath components can be determined using τ_{rms} , which is assumed to be 20 ns, and the minimum path resolution T_p , which is assumed to be 0.5 ns. The average number of resolvable paths, assuming that there is a path every pulse interval, is calculated to be $L = 179$, when all paths whose power is within 15 dB of the strongest one are considered.

In all numerical examples, binary signalling with a data rate of $R_b = 100$ Mbit/s is considered. The receiver is

assumed to have perfect knowledge of the channel coefficients of the first M resolvable paths for all numerical examples, except the one that will be shown in Fig. 10. For the ZF and the ZF-based successive receivers, the signal-to-noise ratio (SNR) per bit is defined as

$$\gamma_b = \frac{E_b}{N_0} \sum_{m=0}^{M-1} e^{-pm}$$

This definition normalises the average power contained in all paths combined by the receiver to unity. For the successive receiver, the SNR per bit is defined as $\gamma_b = E_b/N_0$ because this receiver does not combine the energy contained in multiple resolvable paths.

The error performance of the successive receiver for a system with $N = 4$ (burst repetition interval is $T_r = 40$ ns) is shown in Fig. 4. The error-rate curves of all bits in a burst are provided. It is observed that the first bit has a better performance than the last bit in each burst. This is caused by the error propagation introduced in the interference cancellation process and the slightly higher average power of the first bit.

As mentioned earlier, the last bit has the worst performance and the first bit has the best performance with the ZF receiver. Simulation results are shown in Fig. 5,

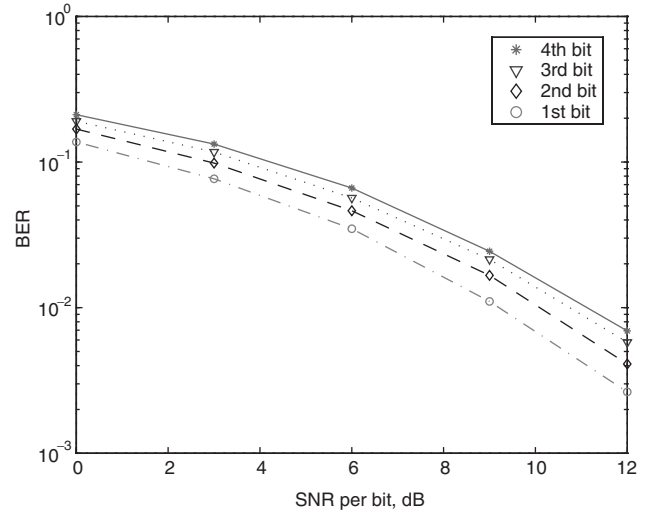


Fig. 4 BER of different bits of a burst against SNR per bit with the successive receiver ($N = 4$)

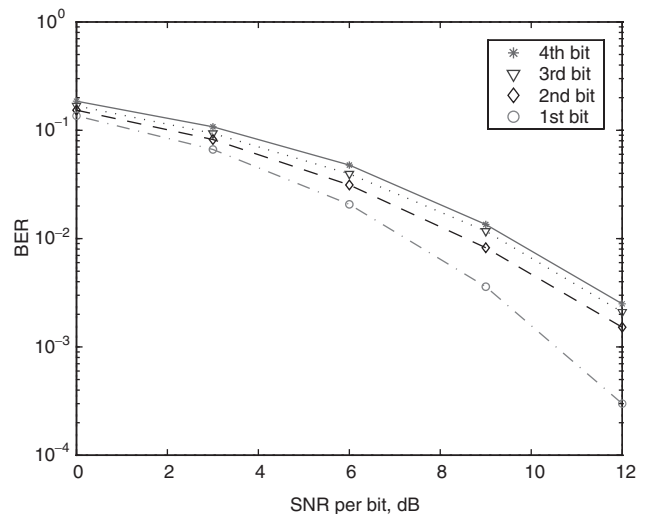


Fig. 5 BER of different bits of a burst against SNR per bit with the ZF receiver ($N = 4, M = 9$)

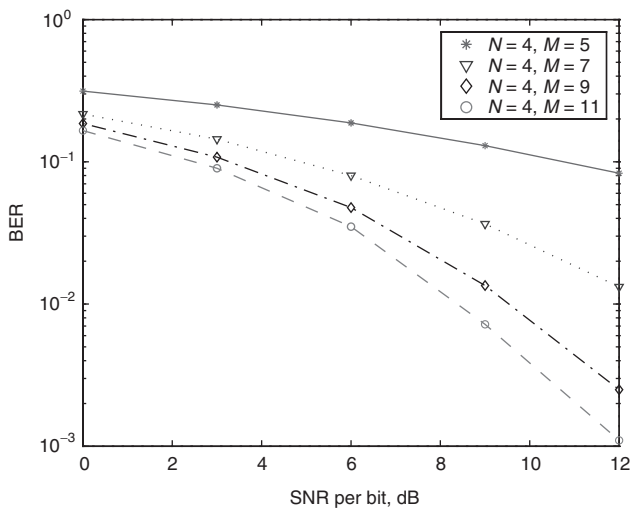


Fig. 6 BER against SNR per bit for the ZF receiver with different values of M ($N=4$)

where $N=4$ bits per burst with $M=9$ samples/burst taken in the receiver. Significant differences in the performance of the first and the last bit of a burst have been observed. Figure 6 shows the impact of the number of paths exploited by the ZF receiver on the error performance of the last bit of each burst. The number of bits per burst for this Figure is fixed at $N=4$. By examining the slopes of the BER curves with different values of $M-N$, it is found that the ZF receiver provides an implicit diversity gain for each bit. Exploiting more resolvable paths results in a higher diversity order for each bit. The non-uniform error performance for different bits in each burst when a ZF receiver is employed is undesirable. However, this problem can be mitigated by combining more paths.

BER curves of different bits of the ZF-based successive receiver are shown in Fig. 7 with $N=4$ and $M=9$. The performance of the first bit is the same as that for the ZF receiver, but the performance of all other bits is much better than for the ZF receiver. Owing to error propagation in the successive cancellation process, the error performance of different bits of a burst still varies slightly with the ZF-based receiver. Figure 8 shows the BER performance of the last bit of a burst with the ZF-based successive receiver. In this Figure, N is fixed at 4 with the number of samples per burst

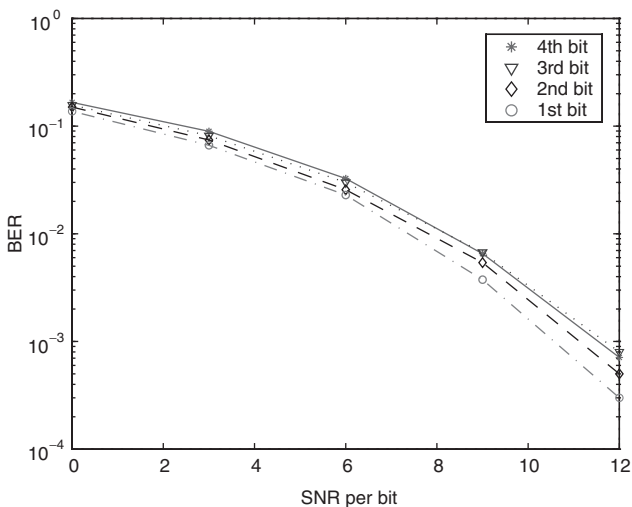


Fig. 7 BER of different bits of a burst against SNR per bit with the ZF-based successive receiver ($N=4$, $M=9$)

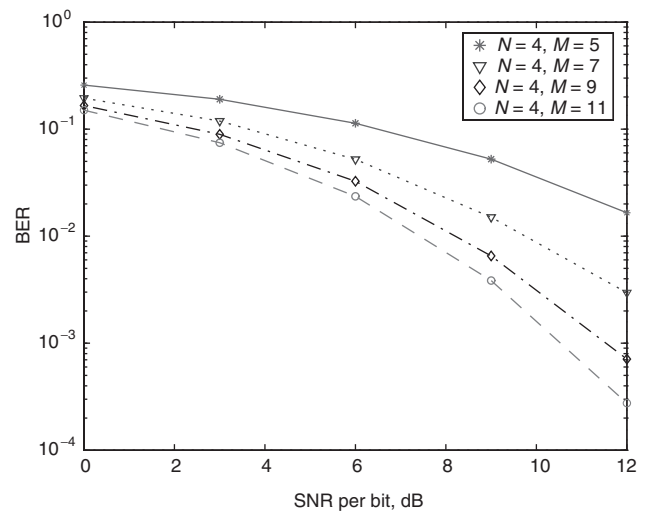


Fig. 8 BER against SNR per bit for the ZF-based successive receiver with different values of M ($N=4$)

M varying. Similar to the ZF receiver, the implicit diversity gain increases as M increases.

A comparison of the BER performance of the last and the first bits of a burst with the successive and the ZF-based successive receivers for the proposed scheme ($N=4$, $M=9$) and a 9-finger RAKE receiver, with maximal ratio combining for the conventional binary pulse amplitude modulation scheme, is given in Fig. 9. As mentioned in the beginning of this Section, the channel delay spread considered is $\tau_{rms}=20$ ns and the system bit rate applied is $R_b=100$ Mbit/s. The normalisation of the channel is done exactly the same way for all cases. The conventional binary PAM scheme exhibits an error floor, which is caused by the excessive amount of inter-symbol interference in the dense multipath environment considered, whereas in the proposed scheme ISI was found to be almost negligible. The proposed scheme with the ZF-based successive receiver performs significantly better than the RAKE receiver for the conventional PAM scheme.

Perfect channel estimates have been assumed for all numerical examples so far. Figure 10 shows the impact of

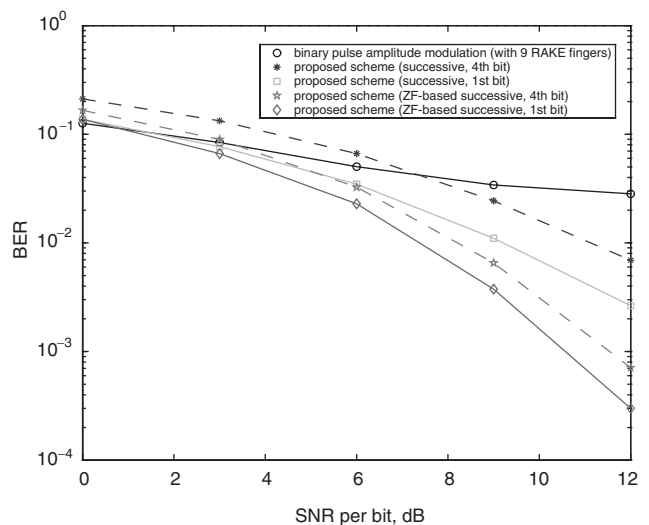


Fig. 9 BER comparison between the conventional binary PAM scheme with a RAKE receiver and the proposed scheme (the last and the first bits of a burst) with the successive and the ZF-based successive receivers ($N=4$, $M=9$, $\tau_{rms}=20$ ns, system operating at a bit rate of $R_b=100$ Mbit/s)

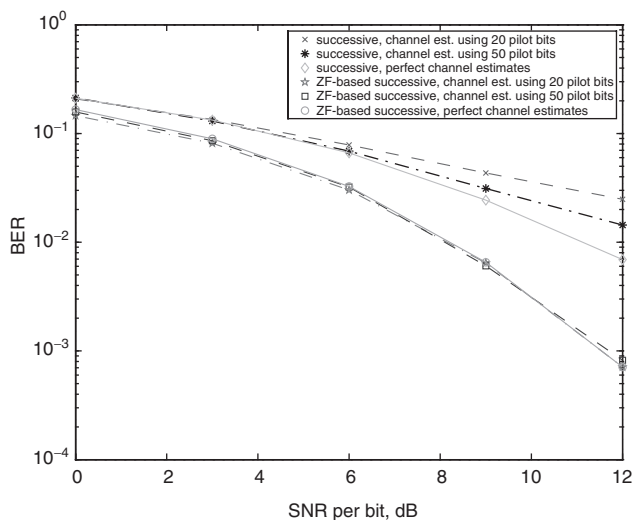


Fig. 10 BER of the last bit of a burst for the successive and the ZF-based successive receivers with actual channel estimates ($N=4$, $M=9$)

imperfect channel estimates on the performance of the successive and the ZF-based successive receivers for the proposed scheme. A quasi-static channel model, that allows the channel coefficients to be constant over a block of 1000 bursts and to change independently from one block to another, is adopted. The channel coefficients for each block are estimated by averaging over 20 and 50 pilot bits. It is observed that imperfect channel estimates affect the successive receiver appreciably. However, the ZF-based receiver with actual channel estimates obtained using 20 and 50 pilot bits performs almost exactly the same as in the case of assuming perfect knowledge of the channel coefficients.

When channel excess delay is the dominating factor that limits the system throughput, the proposed new high-rate scheme could achieve a much higher throughput than the conventional UWB PAM scheme. When the bit duration is much greater than channel delay spread, however, there are no advantages of using the proposed scheme.

5 Conclusion

A new high-rate transmission scheme for pulse-based ultra-wideband systems in dense multipath environments has been proposed. A successive, a zero-forcing and a ZF-based successive receiver have been applied for effective detection in the proposed new scheme. The successive receiver is simple, but it does not provide a diversity gain. The ZF

receiver is more complex than the successive receiver, but an implicit path diversity is achieved when the number of resolvable paths exploited is greater than the number of symbols transmitted in each burst. Although different symbols of a burst have different error performances when a ZF receiver is applied, the gap can be lowered by exploiting more resolvable paths in the receiver. The ZF-based successive receiver works the best. An efficient algorithm that allows the receiver to operate with low computational needs has been derived. Numerical results indicate that the BER performances of all symbols of a burst are nearly the same when the ZF-based successive receiver is employed. Additionally, the ZF-based successive receiver is very robust to channel estimation errors. Given the same channel delay spread, the proposed scheme has the potential to deliver a much higher throughput than the conventional UWB signalling scheme in dense multipath environments.

6 References

- Win, M.Z., and Scholtz, R.A.: 'Impulse radio: how it works', *IEEE Commun. Lett.*, 1998, **2**, pp. 36–38
- Foerster, J.R.: 'The effects of multipath interference on the performance of UWB systems in an indoor wireless channel'. Proc. IEEE Vehicular Technology Conf., Spring 2001, Vol. 2, pp. 1176–1180
- Ho, M., Somayazulu, V.S., Foerster, J., and Roy, S.: 'A differential detector for an ultra-wideband communications system'. Proc. IEEE Vehicular Technology Conf., Spring, 2002, Vol. 4, pp. 1896–1900
- Liu, H.: 'Error performance of a pulse amplitude and position modulated ultra-wideband system in lognormal fading channels', *IEEE Commun. Lett.*, 2003
- Venkatesan, V., Liu, H., Nilsen, C., Kyker, R., and Magaña, M.E.: 'Performance of an optimally spaced PPM ultra-wideband system with direct sequence spreading for multiple access'. Proc. IEEE Vehicular Technology Conf., Oct. 2003
- Zhao, S., Liu, H., and Mo, S.: 'Performance of a multi-band ultra-wideband system over indoor wireless channels'. Proc. IEEE Consumer Communication and Networking Conf. CCNC, Las Vegas, NV, USA, Jan. 2004
- Zhao, L., Haimovich, A.M., and Grebel, H.: 'Performance of ultra-wideband communications in the presence of interference'. Proc. IEEE Int. Conf. on Communication, ICC, Helsinki, Finland, 2001, Vol. 10, pp. 2948–2952
- Win, M.Z., and Scholtz, R.A.: 'On the robustness of ultra-wide bandwidth signals in dense multipath environments', *IEEE Commun. Lett.*, 1998, **2**, pp. 51–53
- Molisch, A.F., Foerster, J.R., and Pendergrass, M.: 'Channel models for ultra-wideband personal area networks', *IEEE Wirel. Commun.*, 2003, **10**, pp. 14–21
- Cassoli, D., Win, M.Z., and Molisch, A.F.: 'The ultra-wide bandwidth indoor channel: from statistical model to simulations', *IEEE J. Sel. Areas Commun.*, 2002, **20**, pp. 1247–1257
- Hashemi, H.: 'Impulse response modeling of indoor radio propagation channels', *IEEE J. Sel. Areas Commun.*, 1993, **11**, pp. 967–978
- <http://grouper.ieee.org/groups/802/15/pub/TG3a.html>
- Falconer, D., Ariyavittakul, S.L., Benyamin-Seeyar, A., and Eidson, B.: 'Frequency domain equalization for single-carrier broadband wireless systems', *IEEE Commun. Mag.*, 2002, pp. 58–66